Magnetization of a $Dy(Fe_{11}Ti)$ single crystal

Bo-Ping Hu, Hong-Shuo Li, and J. M. D. Coey
Department of Pure and Applied Physics, Trinity College, Dublin 2, Ireland

J. P. Gavigan
Laboratoire Louis Néel, Centre National de la Recherche Scientifique, 38042 Grenoble CEDEX, France
(Received 2 August 1989)

Magnetization curves have been measured in the temperature range from 4.2 to 300 K along the [100], [110], and [001] directions of a $Dy(Fe_{11}Ti)$ single crystal in fields up to 7 T. The magnetic moment is along [100] below 58 K and parallel to the c axis above 200 K. Between the two spin-reorientation transitions (first order at 58 K, second order at 200 K) there is a canted spin structure where the net magnetization lies in a (010) plane and is inclined at an angle to the c axis. Three first-order magnetization processes are observed as a function of applied field below 150 K. All the data are used to derive a set of five crystal-field coefficients at the single rare-earth site of the $ThMn_{12}$ structure: $A_{20}=-32.3$ K a_0^{-2}, $A_{40}=-12.4$ K a_0^{-4}, $A_{44}=118$ K a_0^{-4}, $A_{60}=2.56$ K a_0^{-6}, $A_{64}=0.64$ K a_0^{-6}. Spin reorientation observed in the other members of the $R(Fe_{11}Ti)$ ($R\equiv$rare earth) series, except those in $Tb(Fe_{11}Ti)$, are explained by the same crystal-field coefficients.

I. INTRODUCTION

Iron-rich rare-earth intermetallic compounds with the $ThMn_{12}$ structure (space group $I4/mmm$) have been attracting interest as potential permanent-magnet materials. Here we are concerned with developing a systematic understanding of a variety of their intrinsic magnetic properties.

The pure RFe_{12} compound does not exist for any of the rare earths, but the $ThMn_{12}$ structure can be stabilized in pseudobinaries $R(Fe_{12-x}M_x)$, with $M=$Al, Ti, V, Cr, Mo, W, and Si,[1-5] for values of x as low as ~ 1.0. The unit cell is illustrated in Fig. 1. Earlier studies of polycrystalline samples of the $R(Fe_{12}V_2)$ (Refs. 2, 3, and 6–8) and $R(Fe_{11}Ti)$ (Refs. 5 and 9–12) series have established the following points.

(i) The average iron magnetic moment is observed to be about $1.7\mu_B$ at 0 K. Recent theoretical calculations support this value.[13] The compounds appear to be weak ferromagnets.[14]

(ii) Curie temperatures are in the range 480–610 K, with the greatest values for Gd compounds.

(iii) The anisotropy due to the iron sublattice is uniaxial, with $K_1(Fe)=2.0$ MJ m^{-3} for $Y(Fe_{11}Ti)$ (Ref. 11) and $K_1(Fe)=1.7$ MJ m^{-3} for $Y(Fe_{10}V_2)$ (Ref. 2) at 0 K.

(iv) The second-order crystal-field coefficient A_{20} at the $2a$, rare-earth site is negative and considerably smaller in magnitude than -715 k a_0^{-2} found for RCo_5.[15] Values of about -120 K a_0^{-2} have been deduced from the ^{155}Gd electric field gradient in $Gd(Fe_{10}T_2)$ ($T=$V, Mo, and Si) (Ref. 3) and of -60 K a_0^{-2} from analysis of the spin reorientation in polycrystalline $Dy(Fe_{11}Ti)$.[9] This implies that the contribution to the uniaxial anisotropy for those rare-earth ions—Sm^{3+}, Er^{3+}, Tm^{3+}, and Yb^{3+}—having a positive second-order Stevens coefficient α_J is relatively small.

(v) A series of spin-reorientation transitions[9,11,12,16–18] have been found, of which those for the $R(Fe_{11}Ti)$ series are summarized in Fig. 2. These transitions cannot be simply rationalized in terms of the iron anisotropy and that due to the second-order crystal field acting on the rare-earth ions. $Er(Fe_{11}Ti)$,[11,12,18] for example, shows a spin reorientation of the magnetization away from the c axis below 65 K, although both the iron and rare-earth second-order crystal-field contributions to the anisotropy favor the c axis.

To date there are two reports in literature on the magnetic properties of small single crystals of $Er(Fe_{11}Ti)$, $Lu(Fe_{11}Ti)$,[12] and $Sm(Fe_{11}Ti)$.[19] Here we have chosen the $Dy(Fe_{11}Ti)$ compound for detailed investigations. We found earlier that it exhibits two successive spin-reorientation transitions at 80 and 200 K, with a canted spin structure in the intermediate temperature range.[9,11]

The aims of our work have been to determine a complete set of crystal-field coefficients for rare-earth ion in this structure, and to explain thereby the complex magnetic behavior of the $R(Fe_{11}Ti)$ series (Fig. 2). A convenience of the $ThMn_{12}$ structure is the single rare-earth site

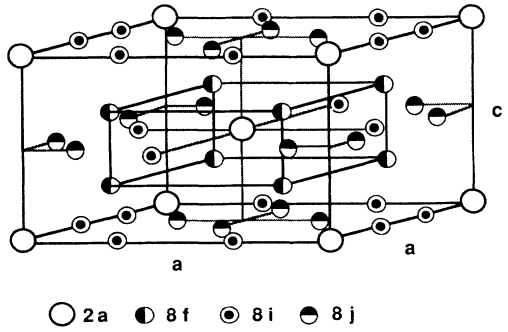

FIG. 1. Crystal structure of $ThMn_{12}$ (space group $I4/mmm$).

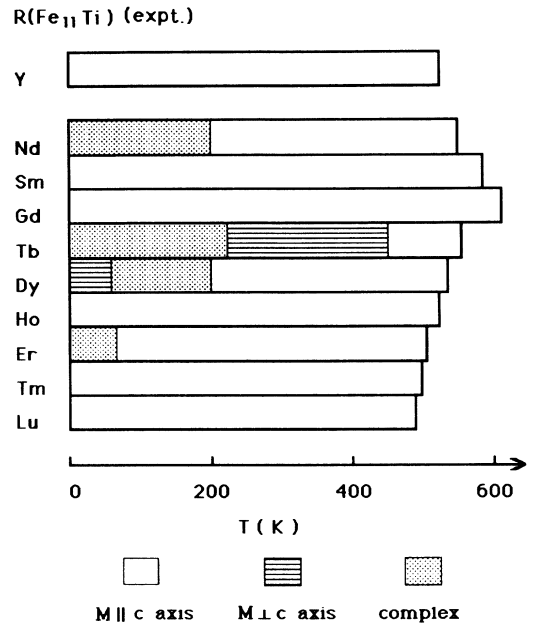

FIG. 2. Observed temperature variation of the magnetic structure of the $R(Fe_{11}Ti)$ series (Ref. 11).

with high uniaxial point symmetry $4/mmm$, needing only five parameters for a complete description of the crystal field. By comparison in the $Nd_2Fe_{14}B$ there are two $mm2$ rare-earth sites, requiring (2)(9)=18 crystal-field parameters.[20]

II. EXPERIMENT RESULTS

The $Dy(Fe_{11}Ti)$ single crystal was prepared by Song-Quan Ji at the Naturrkundig Laboratorium in Amsterdam using the Czochralski method in a tri-arc furnace.[21] The boule, about 40-mm long and 5 mm in diameter, was oriented and cut by spark erosion into three parallelepipeds, each $\sim 3\times4\times4$ mm^3 in size with the faces perpendicular to the principal axes. Magnetization measurements were made in the 7 T extraction magnetometer at the Laboratoire Louis Néel, Grenoble. Magnetization curves were obtained, with field applied along three directions ([100], [110], and [001]), at 17 fixed temperatures from 4.2 to 300 K. All the data were corrected for the demagnetizing field using the initial slopes of the magnetization curves in the easy direction. Some representative curves are shown in Fig. 3.

There is a remarkably large anisotropy at room temperature in the (001) plane between the [100] and [110] directions, which increases as the temperature is lowered. This phenomenon is not observed in other rare-earth transition-metal intermetallic compounds such as in $R_2M_{14}B$ [M=Fe (Refs. 20 and 22) and Co (Ref. 23)] or R_2Co_{17}.[24] Below 58 K, there is a sharp increase of magnetization when a field of 0.5 T is applied along [001]; the magnetization curves thereafter are quite anisotropic. Also, anomalous increases of magnetization are observed when a field of about 1–3 T is applied along [100] or [110], at a temperature in the range 58–150 K. These discontinuities indicate first-order magnetization processes (FOMP's), type I along [100] and type II along [110] and [001], which are similar to those observed, for example in $Nd_2Fe_{14}B$ (Refs. 20 and 25) (type I) and in $Pr_2Fe_{14}B$ (Refs. 26–28) (type II).

From the components of the spontaneous magnetization, M_s, we deduce the temperature variation of the magnitude and orientation of M_s, shown in Fig. 4. The spontaneous magnetization direction is parallel to [100] below $T_1=58$ K, and it is parallel to the c axis above $T_2=200$ K. There is a first-order transition at 58 K to an intermediate orientation in a (010) plane, at an angle $\theta=42°$ from the c axis, and θ then decreases continuously to zero at 200 K. The value of M_s is $10.7\mu_B$ per formula unit at 4.2 K and $11.5\mu_B$ per formula unit at 300 K. The increase of magnetization with increasing temperature is

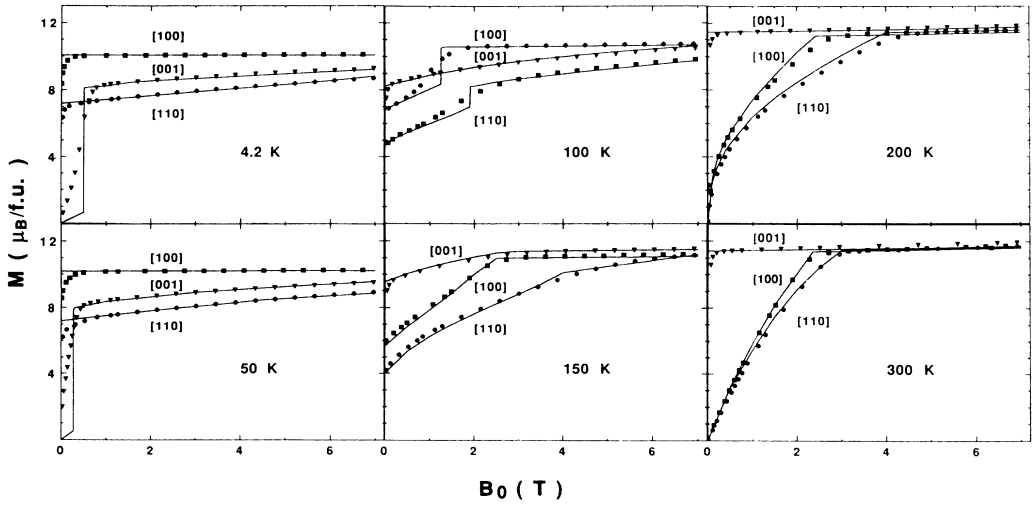

FIG. 3. Experimental (solid symbols) and calculated (lines) single-crystal magnetization curves for $Dy(Fe_{11}Ti)$ compound at six fixed temperatures.

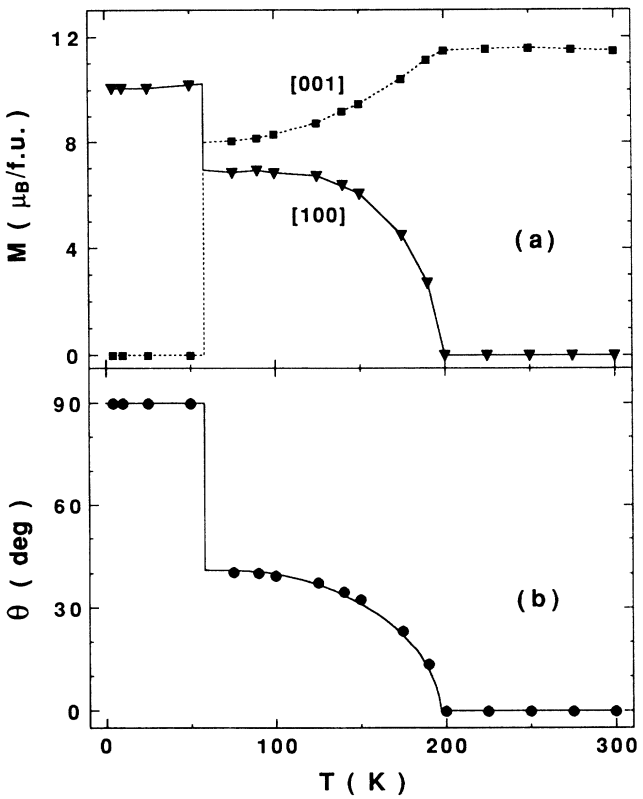

FIG. 4. Temperature variation of the magnitude and the orientation of the spontaneous magnetization M_s: (a) the components of M_s along [100] and [001], (b) the angle θ between the direction of M_s and **c** axis (the line is calculated, see the text).

typical of rare-earth iron intermetallic compounds with a ferrimagnetic structure. The room temperature anisotropy field (average of [100] and [110] directions) is 2.3 T, as reported previously for the polycrystalline material.[11]

III. ANALYSIS OF THE DATA

The method used to analyze the data is the mean-field approximation including exchange and crystal-field interactions, which was originally developed to handle the single-crystal magnetization curves of $Nd_2Fe_{14}B$, and has been fully described elsewhere.[20,29] The model is based on two coupled equations that describe the iron and rare-earth sublattices. The sublattice magnetizations in a $R(Fe_{11}Ti)$ formula are defined as $\mathbf{M}_{Fe}=11\langle\mathbf{m}_{Fe}\rangle$ and $\mathbf{M}_R=\langle\mathbf{m}_R\rangle$, where $\langle\mathbf{m}_{Fe}\rangle$ is the average atomic magnetic moment of the iron and $\mathbf{m}_R=-g_J\mathbf{J}\mu_B$ is the atomic magnetic moment of the rare-earth ion. For the iron sublattice, the energy per formula is given by

$$\mathcal{E}_{Fe}=\mathcal{E}^a_{Fe}-(\mathbf{B}^{ex}_{Fe}+\mathbf{B}^{app})\cdot\mathbf{M}_{Fe}\ , \tag{1a}$$

where

$$\mathcal{E}^a_{Fe}=K_1(Fe)\sin^2\theta_{Fe}$$

and

$$\mathbf{B}^{ex}_{Fe}=-n_{RFe}\gamma\mathbf{M}_R\ [\gamma=2(g_J-1)/g_J]$$

are, respectively, the iron sublattice anisotropy energy and the exchange field acting on the iron magnetization. The intersublattice exchange fields are determined by the exchange coefficient n_{RFe}. For the rare-earth ion, the Hamiltonian is

$$\mathcal{H}_R=\mathcal{H}_{cf}-(\mathbf{B}^{ex}_R+\mathbf{B}^{app})\cdot\mathbf{m}_R\ , \tag{1b}$$

where $\mathbf{B}^{ex}_R=-n_{RFe}\gamma\mathbf{M}_{Fe}$ is the exchange field acting on rare-earth ions (R-R interactions are neglected). The crystal-field Hamiltonian at the rare-earth site is

$$\mathcal{H}_{cf}=B_{20}O_{20}+B_{40}O_{40}+B_{44}O_{44}+b_{60}O_{60}+B_{64}O_{64}\ . \tag{2}$$

(However it must be modified if there is any significant J mixing, e.g., Sm^{3+}.) The $\{B_{nm}\}$ are crystal-field parameters depending on the specific rare-earth ion and $\{O_{nm}(J)\}$ are the Stevens equivalent operators.[30] In the intersublattice exchange energy, $\mathcal{E}_{ex}=n_{RFe}\gamma\mathbf{M}_{Fe}\cdot\mathbf{M}_R$, the factor $\gamma=2(g_J-1)/g_J$ is included because the exchange fields act on the spin magnetic moment of the $4f$ shell and the iron $3d$ shell. In the analysis, the temperature dependence of the iron sublattice magnetization $\mathbf{M}_{Fe}$ and anisotropy constant $K_1(Fe)$ were initially taken to be those of $Y(Fe_{11}Ti)$.[11,31]

The magnetic structure at any given temperature or applied field is determined by solving the coupled Eqs. (1), while minimizing the total energy

$$\mathcal{E}_{tot}=\mathcal{E}_{Fe}+\mathcal{F}_R-\mathcal{E}_{ex}\ , \tag{3}$$

where $\mathcal{F}_R=-k_BT\ln(Z_R)$ is the rare-earth free energy, resulting from direct diagonalization of the rare-earth Hamiltonian, and the last term is included to avoid counting the exchange interactions twice.

A set of $\{B_{nm}\}$ and a value of n_{DyFe} are sought, which allow the magnetization curves of the $Dy(Fe_{11}Ti)$ single crystal to be fitted in a consistent way. A small adjustment ($\sim$5% increase) of M_{Fe} was made to give reason-

TABLE I. Crystal-field parameters B_{nm} (in units of K/ion) obtained from fitting the single-crystal magnetization curves for $Dy(Fe_{11}Ti)$, and the corresponding crystal-field coefficients (in units of K a_0^{-n}): $A_{nm}=B_{nm}/\theta_n\langle r^n\rangle$, $\{\theta_n\}$ are the Stevens coefficients and the values of $\langle r^n\rangle$ were taken from Ref. 34.

B_{20}	B_{40}	B_{44}	B_{60}	B_{64}
0.160	11.0×10^{-4}	-105×10^{-4}	16.0×10^{-6}	4.0×10^{-6}
A_{20}	A_{40}	A_{44}	A_{60}	A_{64}
−32.3	−12.4	118	2.56	0.64

able values of the spontaneous magnetization at low temperature where the exchange interactions do not greatly influence the rare-earth magnetic moment. This increase of iron moment in the dysprosium compound over that for the yttrium compound is in accordance with Mössbauer data for the $R(Fe_{11}Ti)$ series[32] and is also observed in the $R_2Fe_{14}B$ series.[33]

The resulting value of n_{DyFe} is 141 μ_0 and the values of $\{B_{nm}\}$ found are given in Table I, together with the corresponding $\{A_{nm}\}$ values. These parameters give a complete account of the experimental data. The calculated variation $\theta(T)$ is shown by the line on Fig. 4(b); the two calculated spin-reorientation transition temperatures are $T_1^{calc}=58$ K and $T_2^{calc}=197$ K, compared to the experimental values of $T_1=58$ K and $T_2=200$ K. The calculated magnetization curves are also shown by the lines on Fig. 3. Agreement between experiment and calculation is good over the whole temperature range. However a reduction of $\sim 30\%$ of B_{20} (or A_{20}) improves the fit at 300 K.

At low temperature, there are two nearly degenerate energy minima in the total energy surface for the (010) plane, defined by Eq. (3), one at $\theta \approx 40°$ then the other at $\theta_2=90°$, as shown in Fig. 5. When $T<58$ K, the energy is lowest for $\theta=90°$, but as temperature increases ($58<T<200$ K) the energy minimum corresponding to an intermediate angle is lower. This angle decreases with increasing temperature and finally becomes zero when $T \geq 200$ K. The energy levels corresponding to these three cases are presented in Fig. 6, and the resulting ground-state wave functions for Dy^{3+} are given in Table II. (The near degeneracy of the $|\frac{15}{2},\frac{15}{2}\rangle$ ground state and the $|\frac{15}{2},\frac{13}{2}\rangle$ first excited state at 210 K is largely due to the $B_{60}O_{60}$ term in the crystal field.)

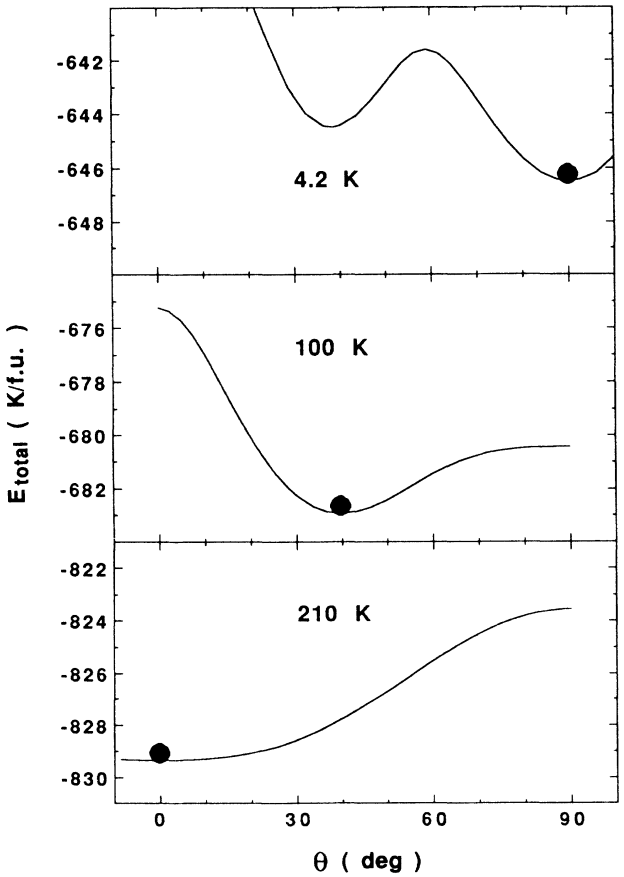

FIG. 5. Calculated energy surfaces in the (010) plane of Dy($Fe_{11}Ti$), nergy minima are: (a) $\theta=90°$ at 4.2 K, (b) $\theta=40°$ at 100 K, and (c) $\theta=0°$ at 210 K, shown by solid circles.

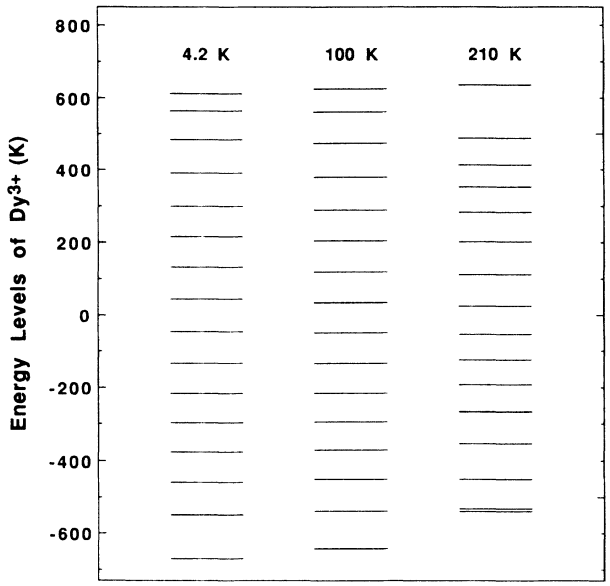

FIG. 6. The calculated energy levels for Dy^{3+} corresponding the three temperatures of Fig. 5, using $n_{DyFe}=141$ μ_0 and the parameters $\{B_{nm}\}$ listed in Table I.

TABLE II. Ground-state wave functions of Dy^{3+}, the corresponding energy levels are shown in Fig. 6. Note that $\Psi_G=\sum_{M=-15/2}^{15/2} C_M|\frac{15}{2},M\rangle$.

C_M (4.2 K)	C_M (100 K)	C_M (210 K)	$\lvert J,M\rangle$
0.0086	0.2693	1.0000	$\lvert\frac{15}{2},\frac{15}{2}\rangle$
0.0318	0.5374	0.000	$\lvert\frac{15}{2},\frac{13}{2}\rangle$
0.0736	0.5629	0.0000	$\lvert\frac{15}{2},\frac{11}{2}\rangle$
0.1324	0.4318	0.0000	$\lvert\frac{15}{2},\frac{9}{2}\rangle$
0.2122	0.2865	0.0000	$\lvert\frac{15}{2},\frac{7}{2}\rangle$
0.3015	0.1824	0.0000	$\lvert\frac{15}{2},\frac{5}{2}\rangle$
0.3851	0.1149	0.0000	$\lvert\frac{15}{2},\frac{3}{2}\rangle$
0.4374	0.0694	0.0000	$\lvert\frac{15}{2},\frac{1}{2}\rangle$
0.4374	0.0387	0.0000	$\lvert\frac{15}{2},-\frac{1}{2}\rangle$
0.3851	0.0198	0.0000	$\lvert\frac{15}{2},-\frac{3}{2}\rangle$
0.3015	0.0094	0.0000	$\lvert\frac{15}{2},-\frac{5}{2}\rangle$
0.2122	0.0042	0.0000	$\lvert\frac{15}{2},-\frac{7}{2}\rangle$
0.1342	0.0017	0.0000	$\lvert\frac{15}{2},-\frac{9}{2}\rangle$
0.0736	0.0006	0.0000	$\lvert\frac{15}{2},-\frac{11}{2}\rangle$
0.0318	0.0002	0.0000	$\lvert\frac{15}{2},-\frac{13}{2}\rangle$
0.0086	0.0000	0.0000	$\lvert\frac{15}{2},-\frac{15}{2}\rangle$

IV. DISCUSSION

The single-ion exchange and crystal-field model already described gives a rather satisfactory fit to the magnetization curves. The decrease of $|A_{20}|$ with increasing temperature is similar to that for $Nd_2Fe_{14}B$.[20] Multipolar interactions, such as the direct or indirect exchange and quadrupolar interactions,[35,36] between rare-earth ions may be responsible for the decrease.

The relationship between the anisotropy of the individual sublattices and the overall anisotropy for a rigidly coupled ferromagnetic structure is straightforward, but when the ferrimagnetic sublattices are not rigidly coupled, canting between the two sublattices will occur.[37] There are contributions to the overall anisotropy resulting from the noncolinearity. We calculate the thermal variation of the overall effective second-order anisotropy constant K_1^{eff} in the (010) plane, as a function of the individual anisotropy constants $K_1(\text{Fe})$ and $K_1(R)$, as well as the canting angle Δ between iron and rare-earth sublattice magnetizations. We write

$$K_1^{\text{eff}} = K_1(\text{Fe}) + K_1(R) + K_1(\Delta) , \tag{4}$$

where $K_1(\Delta)$ denotes the extra contribution due to the canted structure, $K_1(R)$ and K_1^{eff} are obtained directly from diagonalization of the rare-earth Hamiltonian, $\mathcal{H}_R$, in the presence of a perturbing applied field. The results are shown in Fig. 7. We see in the figure that the canting angle Δ decreases when the magnetization approaches the [001], but it reaches the maximum value of $\sim 2.5°$ for intermediate values of θ (see Fig. 4). The value of $|K_1(\Delta)/[K_1(\text{Fe}) + K_1(R)]|$ can exceed 100%, which reaches a maximum around spin-reorientation temperature, 200 K.

A surprising feature of the $ThMn_{12}$ structure is the very small value of A_{20}. It is negative, so the positive α_J ions (Sm^{3+},Er^{3+},Tm^{3+},Yb^{3+}) contribute to the uniaxial anisotropy. Of these, the anisotropy of Sm^{+3} is much greater than that of any of the others. Indeed it is much greater than can be understood with $A_{20} = -32.3\ \text{K}\,a_0^{-2}$. The likely explanation is that J mixing is important in $Sm(Fe_{11}Ti)$.[19,38] Our new value of A_{20} is significantly smaller than the one we had found previously from measurements on polycrystalline samples[9] and it is also smaller than those reported by Buschow *et al.*[3] from a ^{155}Gd

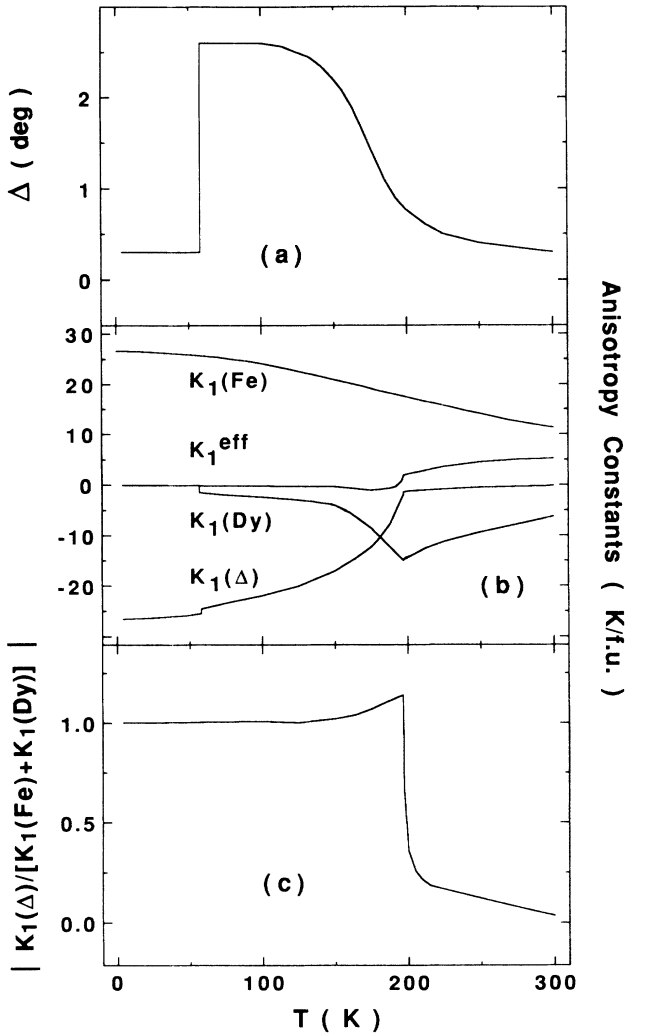

FIG. 7. Temperature variations of (a) the canting angle Δ, (b) the contributions to the second-order anisotropy constant, $K_1(\text{Fe})$, $K_1(R)$, K_1^{eff}, $K_1(\Delta)$, and (c) the ratio of $|K_1(\Delta)/[K_1(\text{Fe}) + K_1(R)]|$, see the text.

Mössbauer study of $Gd(Fe_{10}V_2)$, $-120\ \text{K}\,a_0^{-2}$ and by Moze *et al.*[39] from an inelastic neutron scattering on $ErMn_4Al_8$, $-160\ \text{K}\,a_0^{-2}$. However, recent ^{155}Gd Mössbauer measurements by Czjzek *et al.*[40] on $Gd(Fe_{11}Ti)$ indicate a smaller quadrupole splitting and

TABLE III. Principal component of the electric field gradient V_{zz} and the corresponding second order crystal-field coefficient $A_{20} = -|e|V_{zz}/4(1-\gamma_\infty)$ derived from ^{155}Gd Mössbauer spectroscopy. (γ_∞ is taken to be -92) (Refs. 41–43).

Compound	Structure	V_{zz} (10^{21} V m^{-2})	A_{20} (K a_0^{-2})	Reference
$GdCo_5$	$CaCu_5$	+8.2	−715	15
Gd_2Co_{17}	Th_2Zn_{17}	+4.3	−375	15
$Gd_2Fe_{14}B$	$Nd_2Fe_{14}B$	−7.6	+680	41
$Gd(Fe_{11}Ti)$	$ThMn_{12}$	+0.34	−30	40
$Gd(Fe_{10}V_2)$	$ThMn_{12}$	+1.65	−144	3
$Gd(Fe_{10}Mo_2)$	$ThMn_{12}$	+1.35	−118	3
$Gd(Fe_{10}Si_2)$	$ThMn_{12}$	+1.41	−123	3

give a value of -30 K a_0^{-2}, similar to the one found here. In Table III, we compare the data for a number of rare-earth transition-metal intermetallic compounds.

Scaling the crystal-field parameters obtained from the fitting of $Dy(Fe_{11}Ti)$ and using the values of exchange-field coefficient n_{RFe} deduced from the Curie temperatures (which are roughly twice as large for the light rare earths as for the heavy rare earths),[11] we can predict the magnetic properties for the other rare-earth compounds within the same model. Two puzzling features of the data on Fig. 2 can now be understood, namely the absence of a spin reorientation for $Ho(Fe_{11}Ti)$ and the presence of a spin reorientation for $Er(Fe_{11}Ti)$. For $Ho(Fe_{11}Ti)$, α_J of Ho^{3+} is quite small, so that the second-order term $B_{20}\langle O_{20}\rangle$ is 6.4 K, compared with 16.8 K for Dy^{3+}. The uniaxial anisotrophy of the iron is always great enough to overcome the tendency towards a spin reorientation arising from Ho^{3+}. The calculated energy surface (Fig. 8) shows that the minima at $\theta=0°$ and $\theta=54°$ are almost degenerate, but that at $\theta=0°$ is slightly lower. Weakening of the transition-metal anisotropy by substituting a little cobalt or in $R(Fe_{12-x}M_x)$ with M other than Ti, for example, are expected to lead an intermediate spin reorientation. A spin-reorientation transition, indeed, has been observed in the $Ho(Fe_{10}Mo_2)$ compound at low temperature.[44] In the case of $Er(Fe_{11}Ti)$, the iron and the rare-earth second-order anisotropy both favor the c axis, while $B_{20}\langle O_{20}\rangle=-6.12$ K, $B_{40}\langle O_{40}\rangle=-11.4$ K, and $B_{60}\langle O_{60}\rangle=23.0$ K at 0 K. The spin reorientation below 65 K in $Er(Fe_{11}Ti)$ is actually driven by the sixth-order term $B_{60}\langle O_{60}\rangle$, which is exceptionally large for Er due to its large and positive value of γ_J. A comparable spin reorientation below 60 K in $Er(Fe_{10}V_2)$ was earlier attributed to a large positive $B_{40}\langle O_{40}\rangle$ term.[8] Figure 9 shows the predicted temperature variation of θ for several members of the series, based on the values of A_{nm} obtained for $Dy(Fe_{11}Ti)$. The

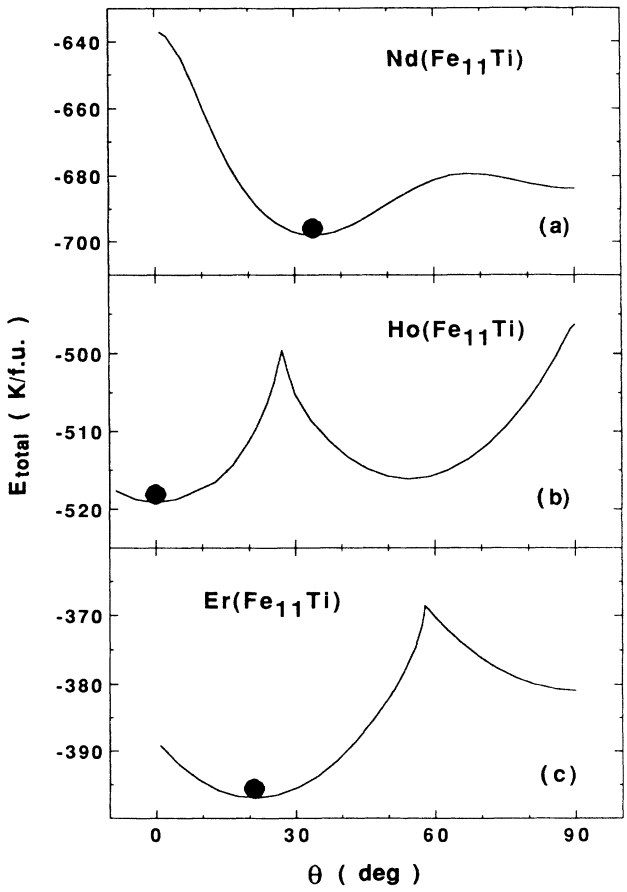

FIG. 8. The calculated energy surfaces at 4.2 K for (a) $Nd(Fe_{11}Ti)$ in the (010) plane, (b) $Ho(Fe_{11}Ti)$ in the (010) plane, (c) $Er(Fe_{11}Ti)$ in the (110) plane.

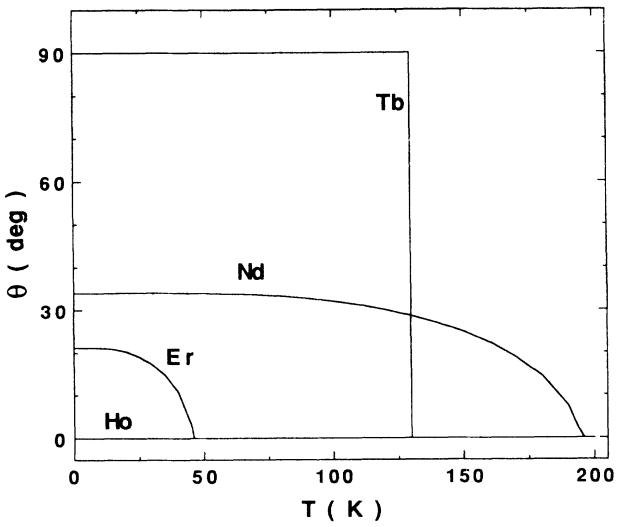

FIG. 9. The calculated temperature variation of the tilting angle θ for $R(Fe_{11}Ti)$ compounds (R =Nd, Tb, Ho, and Er), using the scaled parameters from the fitting of single-crystal magnetization curves of $Dy(Fe_{11}Ti)$. (The variation for Dy is shown in Fig. 4.)

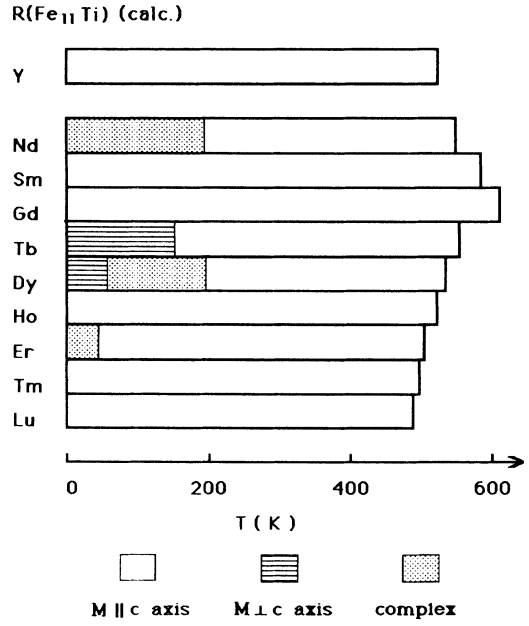

FIG. 10. Calculated temperature variation of the magnetic structure of $R(Fe_{11}Ti)$ series, using parameters scaled from the fit of the single-crystal magnetization curves of $Dy(Fe_{11}Ti)$.

easy magnetization direction in the plane is determined by the fourth-order Stevens coefficient, which is along [100] for Nd, Dy, and Ho ($\beta_J < 0$) compounds and along [110] for Sm, Tb, and Er ($\beta_J > 0$) compounds.

The behavior expected for the $R(Fe_{11}Ti)$ series is also summarized in Fig. 10. Comparison with Fig. 2 shows that the spin reorientation in Nd, Dy, and Er compounds are well reproduced, as is the lack of a spin reorientation for the Ho compound. The only discrepancy is the Tb compound, for which we have no good explanation at present, but it is conceivable that some small admixture of the Tb^{4+} ($4f^7$) state might double the effective $B_{20}O_{20}$ interaction. We have previously found in the $R_2Fe_{14}B$ series that A_{20} behaves anomalously for Pr and Yb,[27] and have attributed this to incipient valence instability.

V. CONCLUSION

We now have a good understanding of the intrinsic magnetic properties of most members of the $R(Fe_{11}Ti)$ series, based on the crystal-field parameters obtained by fitting the single-crystal magnetization curves of $Dy(Fe_{11}Ti)$ over a wide temperature range. The two spin-reorientation transitions observed in this compound, the large in-plane anisotropy and the FOMP's allow us to tie down all the crystal-field parameters with considerable confidence. A comparison of the energy-level schemes developed from magnetization data with those measured independently by inelastic neutron scattering[39] in the same compound should now be made to further validate the approach.

From a practical viewpoint, the small value of A_{20} means that only for $Sm(Fe_{11}Ti)$ is there a significant rare-earth contribution to the uniaxial anisotropy at room temperature. No rare-earth substitution in $Sm(Fe_{11}Ti)$ can increase the anisotropy field. Efforts to develop coercivity and to produce permanent magnets having the $ThMn_{12}$ structure should therefore concentrate on the samarium compound.

The $R(Fe_{11}Ti)$ series provides some nice examples of what happens when the contribution to the anisotropy from the iron sublattice is greater than the second-order anisotropy from the rare-earth sublattice, but is comparable to the higher-order rare-earth terms. In these circumstances, a rich variety of spin-reorientation transitions and canted magnetic structures can appear.

ACKNOWLEDGMENTS

We are very grateful to the Naturrkundig Laboratorium of the University of Amsterdam for providing us with the single crystal of $Dy(Fe_{11}Ti)$. This work forms part of the Concerted European Action on Magnets, a project supported by the Commission of the European Communities.

[1]D. B. De Mooij and K. H. J. Buschow, Philips J. Res. **42**, 246 (1987).
[2]F. R. De Boer, Ying-Kai Huang, D. B. De Mooij, and K. H. J. Buschow, J. Less-Common Met. **135**, 199 (1987).
[3]K. H. J. Buschow, D. B. De Mooij, M. Brouha, H. H. A. Smit, and R. C. Thiel, IEEE Trans. Magn. **MAG-24**, 1161 (1988).
[4]Xian-Zhong Wang, B. Chevalier, T. Berlureau, J. Etouerneau, J. M. D. Coey, and J. M. Cadogan, J. Less-Common Met. **138**, 235 (1988).
[5]Ying-Chang Yang, Lin-Shu Wang, Shu-He Sun, and Dong-Mei Gu, J. Appl. Phys. **63**, 3702 (1988).
[6]K. H. J. Buschow and D. B. de Mooij, *The Concerted European Action on Magnets* (Elsevier, London, 1989), p. 63.
[7]R. B. Helmholdt, J. J. M. Vleggaar, and K. H. J. Buschow, J. Less-Common Met. **138**, L-11 (1988).
[8]O. Moze, P. A. Algarable, M. R. Ibarra, M. Solzi, and L. Pareti, Solid State Commun. **68**, 711 (1988).
[9]Hong-Shuo Li, Bo-Ping Hu, and J. M. D. Coey, Solid State Commun. **66**, 133 (1988).
[10]O. Moze, L. Pareti, M. Solzi, and W. I. F. David, Solid State Commun. **66**, 465 (1988).
[11]Bo-Ping Hu, Hong-Shuo Li, J. P. Gavigan, and J. M. D. Coey, J. Phys. C **1**, 755 (1989).
[12]A. V. Andreev, V. Sechovsky, N. V. Kudrevatykh, S. S. Sigaev, and E. N. Tarasov, J. Less-Common Met. **144**, L-21 (1988).
[13]R. Coehoorn, J. Phys. (Paris) Colloq. **49**, C8-301 (1988); Phys. Rev. B **41** (to be published).
[14]J. M. D. Coey, J. Magn. Magn. Mater. **80**, (1989).
[15]P. C. M. Gubbens, A. M. van der Kraan, and K. H. J. Buschow, J. Phys. (Paris) Colloq. **49**, C8-525 (1988).
[16]P. C. M. Gubbens, A. M. van der Kraan, and K. H. J. Buschow, *Proceedings of the 5th International Symposium on Magnetic Anisotropy and Coercivity in Rare-earth Transition-metal alloys, Bad Soden, 1987* (Deutsche Physikalische Gesellschaft, Bad Honnef, West Germany, 1987), p. 117.
[17]C. Christides, A. Kostikas, D. Niarchos, and A. Simopoulos, J. Phys. (Paris) Colloq. **49**, C8-539 (1988).
[18]Ying-Chang Yang, Lin-Shu Kong, Yuan-bo Zha, Hong Sun, and Xie-di Pei, J. Phys. (Paris) Colloq. **49**, C8-543 (1988).
[19]T. Kaneko, M. Yamada, K. Ohashi, Y. Tawara, R. Osugi, H. Yoshida, G. Kido, and Y. Nakagawa, *Proceedings of the Tenth International Workshop on Rare-earth Magnets and Their Applications, Tokyo, Japan* (The Society of Non-traditional Metallurgy, Kyoto, 1989), p. 191.
[20]J. M. Cadogan, J. P. Gavigan, D. Givord, and Hong-Shuo Li, J. Phys. F **18**, 779 (1988).
[21]A. Menorsky and J. J. M. Franse, J. Cryst. Growth **65**, 286 (1983).
[22]D. Givord, Hong-Shuo Li, J. M. Cadogan, J. M. D. Coey, J. P. Gavigan, O. Yamada, H. Maruyama, M. Sagawa, and S. Hirosawa, J. Appl. Phys. **63**, 3713 (1988).
[23]H. Kato, M. Yamada, G. Kito, Y. Nakagawa, S. Hirosawa, and M. Sagawa, J. Phys. (Paris) Colloq. **49**, C8-575 (1988).
[24]S. Sinnema, Ph.D. thesis, Universiteit van Amsterdam, 1988.
[25]L. Pareti, F. Bolzoni, and O. Moze, Phys. Rev. B **32**, 7604 (1985).
[26]H. Hiroyoshi, H. Kato, M. Yamada, N. Saito, Y. Nakagawa, S. Hirosawa, and M. Sagawa, Solid State Commun. **62**, 475 (1987).

[27]J. P. Gavigan, Hong-Shuo Li, J. M. D. Coey, J. M. Cadogan, and D. Givord, J. Phys. (Paris) Colloq. **49**, C8-557 (1988).
[28]R. Verhoef, J. J. M. Franse, A. A. Menovsky, R. J. Radwanski, Song-Quan Ji, Fu-Ming Yang, Hong-Shuo Li, and J. P. Gavigan, J. Phys. (Paris) Colloq. **49**, C8-565 (1988).
[29]J. M. D. Coey, Hong-Shuo Li, J. P. Gavigan, J. M. Cadogan, and Bo-Ping Hu, *The Concerted European Action on Magnets* (Elsevier, London, 1989), p. 76.
[30]M. T. Hutchings, *Solid State Physics* (Academic, New York, 1964), Vol. 16, p. 227.
[31]Hong-Shuo Li and Bo-Ping Hu, J. Phys. (Paris) Colloq. **49**, C8-513 (1988).
[32]Bo-Ping Hu, Hong-Shou Li, and J. M. D. Coey, Hyperfine Interact. **45**, 233 (1989).
[33]R. Fruchart, P. L'Heritier, P. Dalmas de Réotier, D. Fruchart, P. Wolfers, J. M. D. Coey, L. P. Ferreira, R. Guillen, P. Vulliet, and A. Yaouanc, J. Phys. F **17**, 483 (1987).
[34]A. J. Freeman and J. P. Desclaux, J. Magn. Magn. Mater. **12**, 11 (1979).
[35]P. Morin and D. Schmitt, J. Phys. (Paris) Colloq. **49**, C8-321 (1988).
[36]H. H. Teitelbaum and P. M. Levy, Phys. Rev. **14**, 3058 (1976).
[37]L. Pareti, J. Phys. (Paris) Colloq. **49**, C8-551 (1988).
[38]Hong-Shuo Li, Bo-Ping Hu, J. P. Gavigan, J. M. D. Coey, L. Pareti, and O. Moze, J. Phys. (Paris) Colloq. **49**, C8-541 (1988).
[39]O. Moze, K. H. J. Buschow, R. Osburne, Z. Bowden, and A. D. Taylor, Solid State Commun. **72**, 249 (1989).
[40]G. Czjzek *et al.* (unpublished).
[41]M. Bogé, G. Czjzek, D. Givord, C. Jeandey, H. S. Li, and J. L. Oddou, J. Phys. F **16**, L-67 (1986).
[42]W. A. Barton and J. D. Cashion, J. Phys. C **12**, 2897 (1979).
[43]K. Tomala, G. Czjzek, and H. Schmidt, Solid State Commun. **24**, 857 (1977).
[44]C. Christides, A. Kostikas, D. Niarchos, Hong-Shuo Li, Bo-Ping Hu, and J. M. D. Coey, Solid State Commun. **72**, 839 (1989).

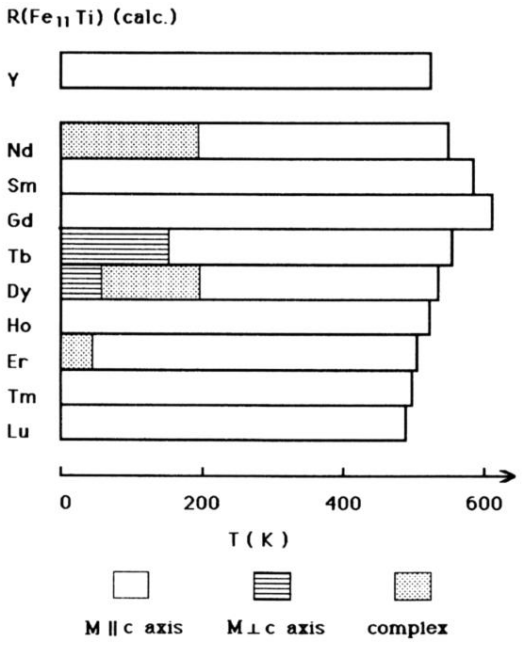

FIG. 10. Calculated temperature variation of the magnetic structure of $R(Fe_{11}Ti)$ series, using parameters scaled from the fit of the single-crystal magnetization curves of $Dy(Fe_{11}Ti)$.

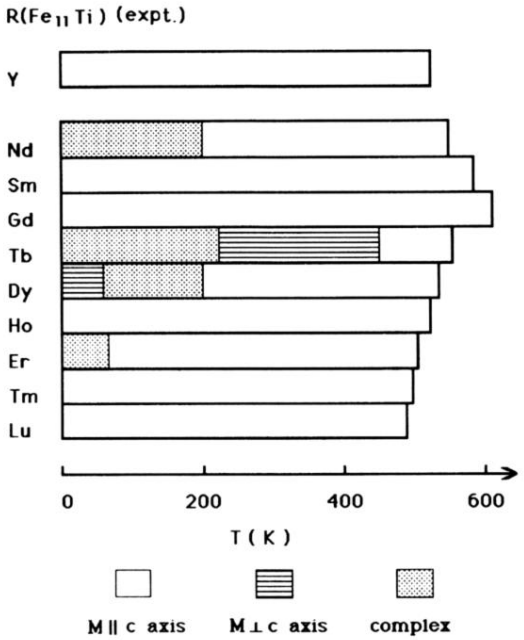

FIG. 2. Observed temperature variation of the magnetic structure of the $R(Fe_{11}Ti)$ series (Ref. 11).